IEEE Access
Multidisciplinary | Rapid Review | Open Access Journal

Received 31 May 2023, accepted 3 July 2023, date of publication 13 July 2023, date of current version 26 July 2023.

Digital Object Identifier 10.1109/ACCESS.2023.3295333

RESEARCH ARTICLE

Provision of Additional Inertia Support for a Power System Network Using Battery Energy Storage System

CHUKWUEMEKA E. OKAFOR AND KOMLA A. FOLLY, (Senior Member, IEEE)
Department of Electrical Engineering, University of Cape Town, Cape Town 7701, South Africa
Corresponding author: Chukwuemeka E. Okafor (OKFCHU002@myuct.ac.za)

This work was supported by the University of Cape Town.

ABSTRACT Battery energy storage system (BESS) will play important roles in the operation of future power systems integrated with high penetration of renewable energy sources. In this work, battery energy storage system (BESS) is equipped with a frequency controller to provide additional inertia support in a power system network made of wind power renewable energy and conventional sources. Several scenarios such as magnitude of power imbalance, transmission line length, variation in wind power penetration level, battery sizing, varying grid inertia were investigated to understand their impacts on the effectiveness of BESS in providing additional inertia support during power system contingencies. Time-domain simulation results of the studied network show that when the transmission line lengths are doubled, the rate of change of frequency (RoCoF) decreased by about 76% resulting in the minimum frequency rising from 49.39Hz to 49.85Hz during the power system disturbance. Besides, by increasing the size of BESS from 50MW to 130MW, the RoCoF was improved from −0.43876Hz/s to −0.30668Hz/s thereby raising the minimum frequency from 48.98Hz to 49.67Hz. Further results from the simulations show that when the magnitude of power imbalance was increased from 150 MW to 375MW, the BESS could not effectively provide additional support as the output power from the power converter remained fairly constant at about 60MW.

INDEX TERMS Battery energy storage system (BESS), frequency response, inertia response, rate of change of frequency (RoCoF), wind power.

I. INTRODUCTION

The power system has undergone massive transformation in recent years. Prominent among this transformation is the structural change in the power system network with a massive deployment of renewable-based power plants (i.e., wind and solar power plants) resulting in the reduction in the number of the conventional power plants (CPPs). The CPPs are mainly operated by fossil-fuels which are highly environmentally unfriendly. The renewable energy sources (RESs) have little or no adverse effects on the environment and have a high economic value although they are not dispatchable [1]. Other technical challenges that may arise with increased penetration of these renewable energy sources include low fault ride through capability, increased degree of uncertainty, a decrease in generation reserve and poor quality of power produced [2].

It is well-known that CPPs which are synchronous generator based can naturally release inertia to sudden change in frequencies [3], [4], however, this is not the case with inverter based RESs. The connection of RES-based plants to the power grid is through electronic power converter interface thereby the grid frequency is decoupled from the rotational speed of the machines. Therefore, integrating inverter-based RES plants in a massive proportion could lead to reduced grid inertia [4], thereby creating frequency stability issues due to high rate of change of frequency (RoCoF) [4], [5]. In the literature, many new controllers have been designed to ''imitate'' the behavior of the synchronous-based generator for better system frequency response. Some of these controller-based techniques are de-loading technique, inertia response (IR) method, droop control method and energy

The associate editor coordinating the review of this manuscript and approving it for publication was Vitor Monteiro.

storage technique [2]. The de-loading technique utilizes the wind's capability of making provision of reserve power to mitigate the deviations in the frequency [2], whereas in the inertia response method, the stored kinetic energy in the rotating masses is released through the help of special controllers [6]. In the droop controller method, the output power is adjusted in line with the changes in the system frequency according to the setting of the droop. Energy storage systems have been successfully deployed for inertia support as presented in [7] and [8] and for primary frequency regulation [9]. The energy storage technique of producing additional inertia support involves the use of controllers to enable the controlled discharge of the energy storage system [1]. Frequency controllers and active power injectors are used to produce synthetic inertia from BESS [1], [5].

Frequency response according to [1] and [7] is categorized into inertial response, primary frequency control (PFC), secondary frequency control (SFC) and tertiary frequency control (TFC). The three main indicators used in the study of power system frequency response are the frequency nadir (the minimum frequency), the steady state frequency, and rate of change of frequency (ROCOF) [4], [5], [6]. The primary and the secondary frequency control are provided by the turbine governor and automatic generation control (AGC), respectively. According to [9], there are two fast responses that make up the primary frequency control. These are the inertia response and the governor control. The governor control can be made available by ensuring that the active power provided by the dispatched online generators are sufficiently increased while the IR is continuously getting reduced because of the increased non-synchronous generation sources such as wind and solar photovoltaic [10], [11]. IR is primarily due to the stored kinetic energy in rotating masses of load motors and synchronous generators. In the case of any power system contingencies, this kinetic energy is released to compensate for the change and keeps the system from going under limits [4], [12]. Thus, IR is a fast frequency response, and plays a key role in power system stability especially during the initial stage of a frequency event in power system. When non-synchronous generation sources are connected via converters to the grid, they do not naturally contribute inertia to the grid but could be enabled through appropriate controllers to produce inertia called emulated or synthetic inertia [4], [5].

Energy storage systems with fast response time could be used to provide for declining inertia [13]. The main reasons for the integration of these storage devices in power system is because of the need to meet the necessary balance between production and usage of electricity and for the maintenance of the required power quality despite the intermittency of these weather -based power generations [14]. In considering the feasibility of these energy storage devices for application in the grid, the applications technical requirements such as response time, power and energy capacities are of utmost importance. Energy storage systems suitable for inertia support in the grid includes battery energy storage, flywheel, supercapacitors, etc. This is due to their noticeably short response times (in milliseconds) and higher power capacities.

Considering the works in the literature, several authors have done extensive research on enabling inertial response from BESS. The impacts of the magnitude of power system disturbance, and system robustness, have been examined to some extent [1]. However, to the best of our knowledge, nothing has been done on how transmission line length affects the rate of change of frequency during power system contingency and also how the magnitude of power system disturbances affects the effectiveness of BESS in providing additional inertia support during contingencies.

The main contributions of this paper are summarised as follows:

- The study brought to light the impacts of transmission line lengths in the effectiveness of BESS providing frequency support during power system contingency. This should be taken into consideration in the sizing of BESS for inertia support in a transmission network in order to avoid over-sizing of the BESS due to the inherently low RoCoF of longer transmission lines.
- Moreover, the work reveals that BESS may be ineffective in providing inertia support once the converter maximum output power is exceeded. This is very critical because at that level (when the maximum output power of the converter is attained) the output active power injected by BESS will remain fairly constant despite further increase in the size of the disturbance, thus making BESS to become ineffective in providing additional inertia support to curtail frequency deviations.

It should be mentioned that the simulations in this paper are carried out using DigSILENT Power Factory.

The paper is structured as follows: section II introduces details of inertial response controllers for BESS. Section III presents overview of the BESS's controllers used in this work for enabling inertia response. The power system model used for this study as implemented in DIgSILENT Power factory is presented in Section IV while the methodology deployed for the work is given in Section V. Simulations results are discussed in Section VI while conclusion forms the content of the last section.

II. INERTIAL RESPONSE CONTROLLERS FOR BESS

The power system frequency changes continuously and its derivative shows the balance between consumed and produced electricity [5]. In the event of power system disturbance, the balance between generation and demand will be lost and the system frequency will respond at a rate initially determined by the total system inertia [15]. The total system inertia is the sum of all the kinetic energy stored in the rotating masses of all the machines connected to the grid. In the case of contingency, for example sudden large load increase, the system inertia will be injected into the grid as fast active power to compensate for the loss in the generated power, In the case that the system inherent inertia is insufficient,

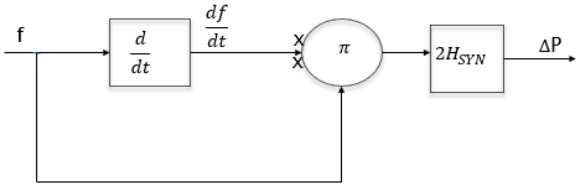

FIGURE 1. Block diagram of the frequency controller [17].

energy storage systems and power sources that are integrated into the grid could be enabled (through the use of full-rated power converter) to produce synthetic inertia [16], [17]. For BESS, synthetic inertia can be produced when the battery is discharged in a controlled manner to provide an additional inertial power [4], [15].

A. FREQUENCY/INERTIA CONTROLLER

The inertia controller could be described as a simple loop that increases the active output power of the power converter at the early stages of a significant under frequency event [4]. It activates the discharge of BESS in a controlled manner producing an additional inertia support with power that could be evaluated using the equivalent of the swing equation of a synchronous machine as given in (1) [16], [18], [19]:

$$\Delta P = 2fH_{SYN}\frac{df}{dt} \tag{1}$$

where ΔP is the load generation imbalance in MW, f is the frequency in Hz, $\frac{df}{dt}$ is the rate of change of frequency (ROCOF) in Hz/s and H_{SYN} is the synthetic inertia in second (s).The block diagram of the frequency controller is shown in Fig 1.

The synthetic inertia (H_{SYN}) represents the gain of the frequency controller [2]. The gain of the frequency controller affects the rate of the discharge of the BESS. When the inertial controller gain is high, the BESS discharges quickly producing excessive heat built-up (thermal runaway) and may degenerate into a second frequency disturbance event because of the drop in the BESS power injection [6], [15]. However, by increasing the synthetic inertia, the inertial response is improved, and a better frequency support is realised [20].

B. FAST ACTIVE POWER CONTROLLER

The fast active power injection/absorption (FAPIA) controller is a frequency response model in the modern power converter [5], [21]. During under frequency event in power system, FAPIA could be used to inject active power to the system or to take out active power from the system for an over frequency condition [22]. The control actions used in this frequency response model are the proportional and derivative control actions [22]. The derivative control is proportional to the rate of change of frequency (ROCOF) as given in (2) [22], [23], [24].

$$\Delta P_{inj/abs} = K_d\frac{df}{dt} \tag{2}$$

where K_d represents the gain of the derivative controller, and f is the measured frequency and $\Delta P_{inj/abs}$ represents

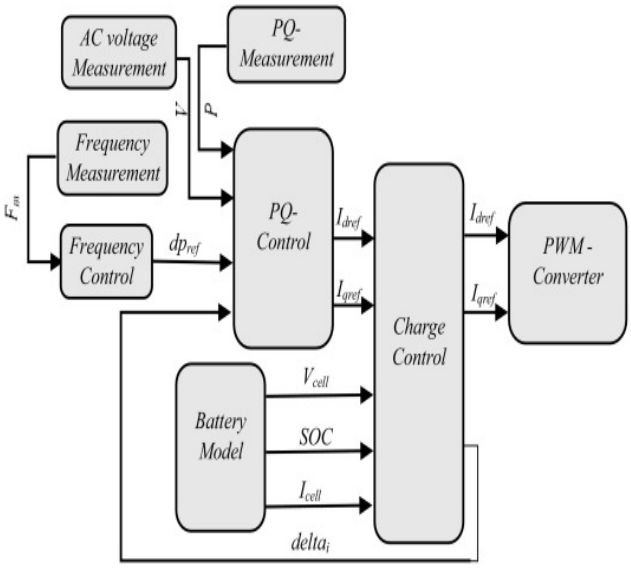

FIGURE 2. BESS model [7], [26].

the injected/absorbed power by the FAPIA controller. The dynamic performance of both control actions can be combined as shown in (3) according to [5] and [21].

$$\Delta P_{inj/abs} = K_p\Delta f - K_d\frac{df}{dt} \tag{3}$$

where,

$$K_p = (\frac{2K_d}{\Delta f})(\frac{df}{dt})$$

where K_p represents the gain of the (K-f) control of the FAPIA controller and the term K_d denotes the inertial contribution of the active power. The effect of K_d term is equivalent to an increase in system's kinetic energy; therefore, it reduces the initial RoCoF [5], [22].

III. OVERVIEW OF A BESS MODEL FOR INERTIA SUPPORT

The Battery energy storage model developed by DIgSILENT Power Factory has been used in many studies relating to frequency stability [17]. This model has been adopted for this work and the details can be found in [25]. Fig 2 shows a block diagram of this model which consists of a battery bank, a frequency controller, a charge controller, an active/reactive power controller and a converter. These subunits are discussed as follows:

A. BATTERY MODEL

The battery model described in [25] which is lithium-ion based is used in this work. It is a double polarization model. The block diagram is shown in Fig 3a, where

R_O is the internal resistance of the battery cell,
R_{TS} is the separation polarization process resistance,
K is the number of cells in parallel,
SoC_0 is the initial state of charge,
R_i is the cell internal resistance,
C_bat is the battery capacity,

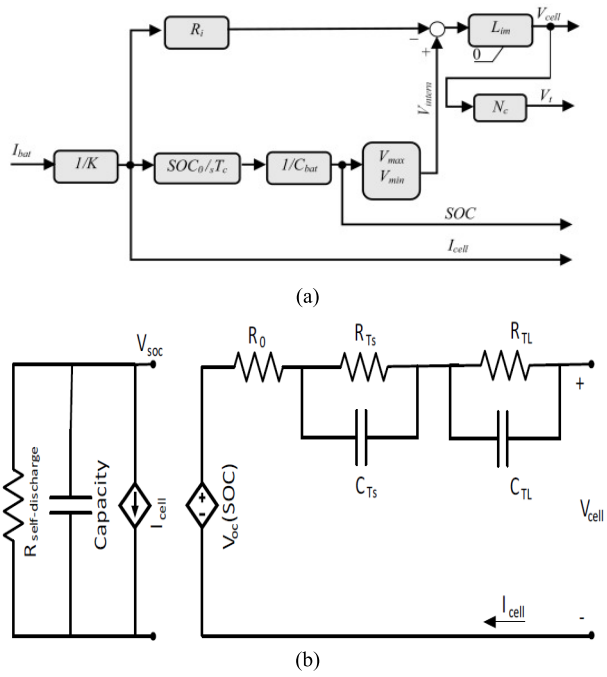

FIGURE 3. (a) Block diagram of the battery model [25]. (b) Equivalent circuit of a battery cell.

Lim is the limiter,
V_{cell} is the terminal voltage of cell,
$\frac{1}{sTc}$ is the integrator with time constant,
$V_{\max}$ is the maximum voltage of the cell,
$V_{\min}$ is the minimum voltage of the cell,
Ns is the number of cells in a string,
I_{bat} is the battery rated current,
Vt is the terminal voltage of the battery,
V_{nom} is the voltage rating of the connected DC-busbar,
I_{cell} is the rated current of a single cell,
SOC is the state of charge,
C_{TS} is the separation polarization process capacitance,
R_{TL} is the electrochemical polarization process resistance,
C_{TL} is the electrochemical polarization process capacitance,
V_{OC} is the open circuit voltage of the cell,
R_{SD} is the self-discharge resistance.

These parameters of the equivalent circuit depend on the state of charge (SoC). The state-of -charge estimation is given by (4),

$$\text{SoC} = \text{SoC}_0 - \frac{1}{C_{cell}} \int_0^t I_{cell}\, \text{dt} \tag{4}$$

where, SoC_0 is the initial state of charge, C_{cell} is the capacity of the battery cell and I_{cell} is the rated current of the single cell. Once the SoC is found from (4), the other parameters of the equivalent circuit can be obtained. From Fig 3b, the terminal voltage of the cell is evaluated as in (5)

$$V_{cell} = V_{oc} - I_{cell}R_0 - U_{TS} - U_{TL} \tag{5}$$

The charging/discharging current can be obtained from the separation polarization process or the electrochemical polarization process. Thus,

$$I_{cell} = \frac{U_{TS}}{R_{TS}} + C_{TS}\frac{dU_{TS}}{dt} \tag{6}$$

where, U_{TS} is the separation polarization process voltage.

Then,

$$\frac{dU_{TS}}{dt} = \frac{I_{cell}}{C_{TS}} - \frac{U_{TS}}{R_{TS}C_{TS}} \tag{7}$$

Similarly,

$$I_{cell} = \frac{U_{TL}}{R_{TL}} + C_{TL}\frac{dU_{TL}}{dt} \tag{8}$$

$$\frac{dU_{TL}}{dt} = \frac{I_{cell}}{C_{TL}} - \frac{U_{TL}}{R_{TL}C_{TL}} \tag{9}$$

where, U_{TL} is the electrochemical polarization process voltage. Considering a complete battery pack, the number of cells in a string, n_s is given by (10)

$$n_s = \frac{U_{batt}}{V_{cell}} \tag{10}$$

where U_{batt} is the DC voltage level of the battery.

Knowing the power requirement of the battery (P_{batt}), the battery rated current (I_{batt}) could be calculated using (11).

$$I_{Batt} = \frac{P_{batt}}{U_{batt}} \tag{11}$$

The number of strings that must be connected in parallel (n_P) to obtain the rated of the battery is provided in (12)

$$n_p = \frac{I_{batt}}{I_{cell}} \tag{12}$$

where, I_{cell} is the rated current of a single cell.

TABLE 1. Battery model parameters [26].

Parameters	Value
State of charge at initialization (SoC_0)	0.8
Cell capacity per cell (Ah)	80
Minimum voltage of cell (V)	12
Maximum voltage of cell (V)	13.8
Number of parallel cells	60
Number of cells in row	65
Cell internal resistance per cell (ohm)	0.001

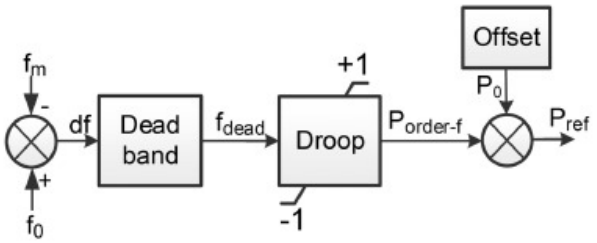

FIGURE 4. Frequency controller [27].

TABLE 2. Frequency controller parameters [26].

Parameter	Value
Droop	0.004
Dead band for frequency control (pu)	0.0002

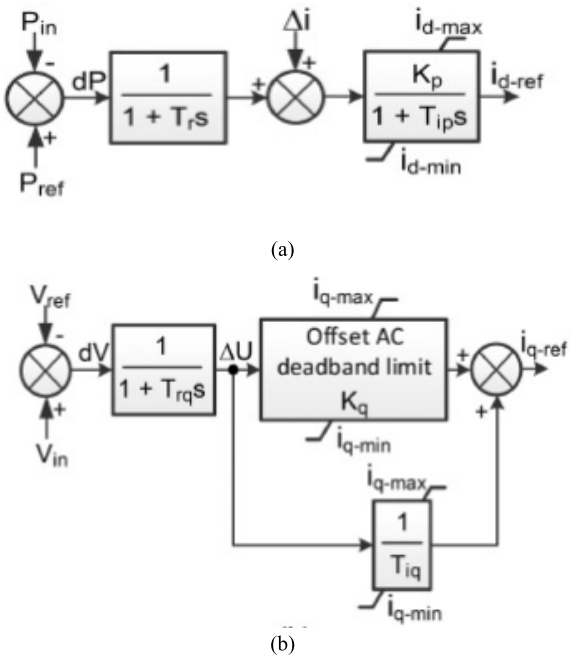

FIGURE 5. (a) PQ controller (active part). (b) PQ controller (reactive power part) [26].

A detailed modelling of the battery is provided in [25] and the values of the circuit parameters are given in Table 1.

B. FREQUENCY/INERTIA CONTROLLER

The block diagram of the frequency controller for BESS is shown in Fig 4. It consists of the frequency control and the frequency droop. The frequency control depends on the rate of change of frequency (RoCoF). The frequency droop coefficient is calculated using (13)

$$R_{droop} = \frac{1}{K_{droop}} = \frac{\Delta f}{\Delta p} \tag{13}$$

Δp is the active power change of the battery and it is determined by R_{droop}, where K_{droop} is the frequency droop and Δf is the change in frequency. The output of the frequency droop/RoCoF controller loop is an active power change signal for the PQ controller [8]. For under frequency contingency it will be positive, and the BESS will switch to discharging mode and for over frequency event, it will be negative, and the BESS will switch to charging mode. The active power change is related to RoCoF according to (14),

$$\Delta p = K_{rocof} \frac{df}{dt} \tag{14}$$

where K_{rocof} is slope of the frequency change.

The frequency controller enables a controlled discharge of the battery. It serves as a simple loop that increases the electrical active power output of the power conversion system during a frequency disturbance event and is calculated using the equivalent swing equation of a synchronous generator according to [4] and [8] as given in (1). More detailed modelling of the inertia controller used in BESS model in DIgSILENT Power Factory could be found in [25] and [26] and the model parameters are given in Table 2.

TABLE 3. PQ controller parameters [26].

Parameters	Value
Filter time constant (active part) Tr (s)	0.01
Filter time constant (reactive part) Trq (s)	0.1
Proportional gain, K_P (pu)	2.0
Proportional gain, Kq (pu)	1.0
Integration time constant, T_{ip}(s)	0.2
Integration time constant, T_{iq}(s)	0.002
Minimum discharging current, $i_{d\ min\ (pu)}$	-0.4
Maximum discharging current, $i_{d\ max\ (pu)}$	1.0
Minimum reactive current, $iq_{\ min\ (pu)}$	-0.1
Maximum reactive current, $iq_{\ max(pu)}$	1.0

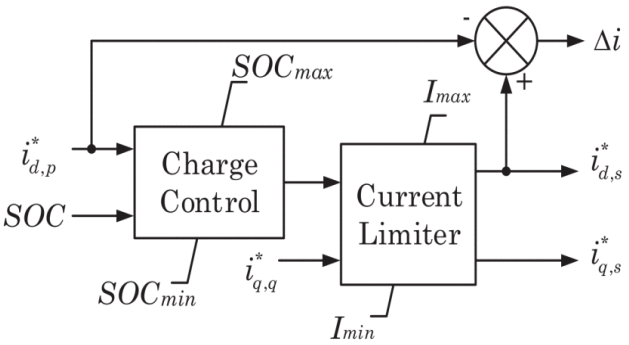

FIGURE 6. A charge controller model [26].

C. PQ CONTROLLERS

The controllers for the active and the reactive power are known as the PQ controllers as shown in Fig 5a and Fig 5b respectively. It is defined in the dq axis current reference. The input signals to the PQ controller are the reference power from the frequency controller (P_{ref}), the ac power and voltage P_{ac} and U_{ac} from the grid. Two loops are in this block. One control loop for the active power and the other for the reactive power control. The dq current signals for the charge controller are produced from the PQ controllers. The model parameters for the PQ controllers are as given in Table 3.

D. CHARGE CONTROLLERS

The model of the battery charge controller consists of two parts, namely the charging logic and the current limiter. The purpose of the charge controller is to achieve the boundary conditions of the battery storage such as the state -of- charge (SOC), minimum and maximum cell voltage. The dq current reference from the charge controller ($I_{d(s)}$ $I_{q(s)}$) is used in controlling the power converter. The block diagram of the charge controller model is shown in Fig 6 while the charge controller model parameters are as given in Table 4.

TABLE 4. Charge controller parameters [26].

Parameters	Value
Minimum charging current (pu)	0.05
SoC_{min} (pu)	0
SoC_{max}	1
Delta (Δi)	0.9

TABLE 5. Transformer data for modified 12-bus system [10].

From -to -Bus	Type	MVA Capacity
1-7	Autotransformer	500
1-9	Step-up	800
2-10	Step -up	700
3-8	Autotransformer	500
3-11	Step-up	400

TABLE 6. Conventional power plants (CPPs) for the modified 12-bus system [10].

CPP	Capacity (MVA)
G1	750
G2	640
G3	474

TABLE 7. Line data for the modified 12-bus system [10].

Line	Length (L) in km	R(PU)	X(PU)
1-2	100	0.01131	0.18377
1-6	300	0.33940	0.55130
2-5	400	0.04530	0.73510
3-4	100(x2)	0.02262	0.36750
4-5	150	0.01700	0.27570
5-6	300	0.03394	0.55130
7-8	600	0.06788	1.10260

E. POWER CONVERTER SYSTEM

A power converter system transforms the direct current (DC) voltage from the storage unit into the alternating current (AC) voltage required in the power network. The converter is equipped with appropriate controllers to help it perform specific functions and interfaces the energy storage device and the grid. The power converter is controlled using the dq axis current reference from the charge controller. The output signals from the power converter are the ac power (P_{ac}) and ac current (I_{ac}).

IV. TEST SYSTEM MODEL

Figure 7 shows a modified 12-bus test model with system frequency of 50Hz. The original 12-bus system in [10] has been modified by two wind power plants at buses 3 and 4 and a battery energy storage at bus 12. The maximum and minimum frequency limits are 51Hz and 48.75Hz respectively [27]. Table 5 to Table 9 are the summary of the network parameters.

TABLE 8. Bus data for 12-bus system [10].

BUS	V (kV)	Type	Load (MW), pf	P_{gen} (pu)	V mag (pu)
1	230	PQ	300, 0.85 lag	-	-
2	230	PQ	250, 0.90 lag	-	-
3	230	PQ	350, 0.95 lag	-	-
4	230	PQ	300, 0.85 lag	-	-
5	230	PQ	100, 0.90 lag	-	-
6	230	PQ	150, 0.95 lag	-	-
7	345	PQ	-	-	-
8	345	PQ	-	-	-
9	15.5	SL	-	-	1.00
10	15	PV	-	4.0	1.01
11	13.8	PV	-	3.3	1.01

TABLE 9. Wind power plant and bess parameters.

Energy sources	Power capacity (MVA)	Number of units	Bus of connection
BESS	90	1	1
Wind power plant	250	2	3 and 4

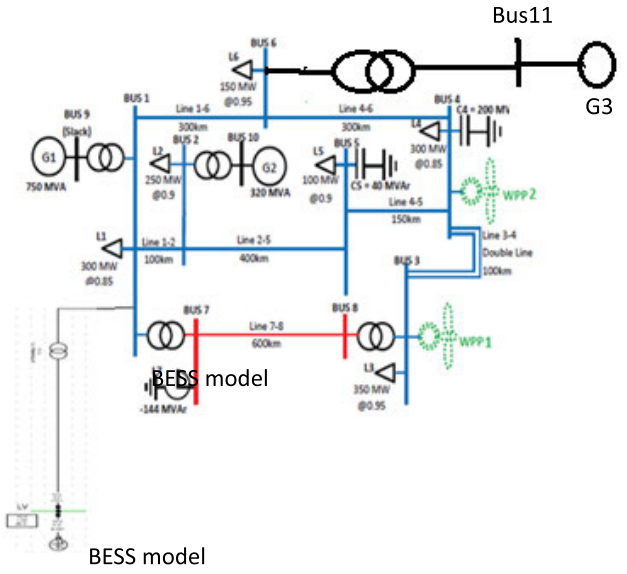

FIGURE 7. Modified 12-Bus test system model.

V. METHODOLOGY

This work investigates the effectiveness of BESS in providing inertia support in a grid network during a power system contingency. The test system and its parameters were provided in Section IV. The BESS model described in [25] is deployed and the whole network (Fig 7) modelled using DIgSILENT Power Factory for the demonstration of the simulations and

for the study of the impacts of BESS in supplying additional inertia support for frequency stability during system frequency events. Several scenarios (such as variation in transmission line lengths, variation in wind output power, battery sizes and varying grid inertia) were investigated to understand their impacts on the effectiveness of BESS in providing additional inertia support during contingencies.For every of these grid conditions, the test system is simulated for 10 seconds with the activation of a power system contingency event at 5 seconds after the commencement of the simulation. The simulations are in two phases. The first phase is without BESS providing additional inertia support while the second phase is with BESS providing additional inertia support. Thereafter, the impacts of BESS are examined by studying the frequency nadirs and the rate of change of frequency attained during the simulations.

VI. SIMULATIONS AND RESULTS

The modelling and simulation of the modified 12-bus test system was carried out in the DIgSILENT Power Factory environment with the purpose of enabling the battery energy storage to produce inertia response for frequency support during a sudden load change. According to [2], the most severe case of load increase for the test system model is 300MW. After five seconds of starting the simulation, a 300MW load increase was activated. The total time for the simulation is 10 seconds. The frequency response indicators used in this work are the minimum frequency (reached during the 10seconds simulations) and the rate of change of frequency (ROCOF) at 200 milliseconds time window. Simulation results were obtained considering the following scenarios:

A. EFFECTS OF USING BESS FOR ADDITIONAL INERTIA SUPPORT DURING A SUDDEN LOAD INCREASE OF 300MW ON THE SYSTEM

The purpose of this simulation is to investigate the effectiveness of BESS in providing inertia support and improving frequency stability during a power system contingency of sudden load increase. The load increase was activated 5s after the commencement of the simulation and the total simulation time was 10 seconds.

1) MINIMUM FREQUENCY

The minimum frequency reached during the load frequency event is one of the indicators of the frequency response of the system during contingency. In the frequency response curves shown in Fig. 8, the minimum frequencies attained during the 300MW sudden load increase (at 5seconds after the start of the simulation) are 47.19Hz when the BESS is not in operation and 49.18Hz when the BESS is operating. This shows that the BESS has helped in preventing the frequency from falling to a level that may result in underfrequency load shedding. This is because of the active power supplied by the BESS during the sudden load increase as shown in Fig. 9. At the instant of the 300MW load increase, that is

FIGURE 8. Frequency response plot with and without BESS (300 MW load increase).

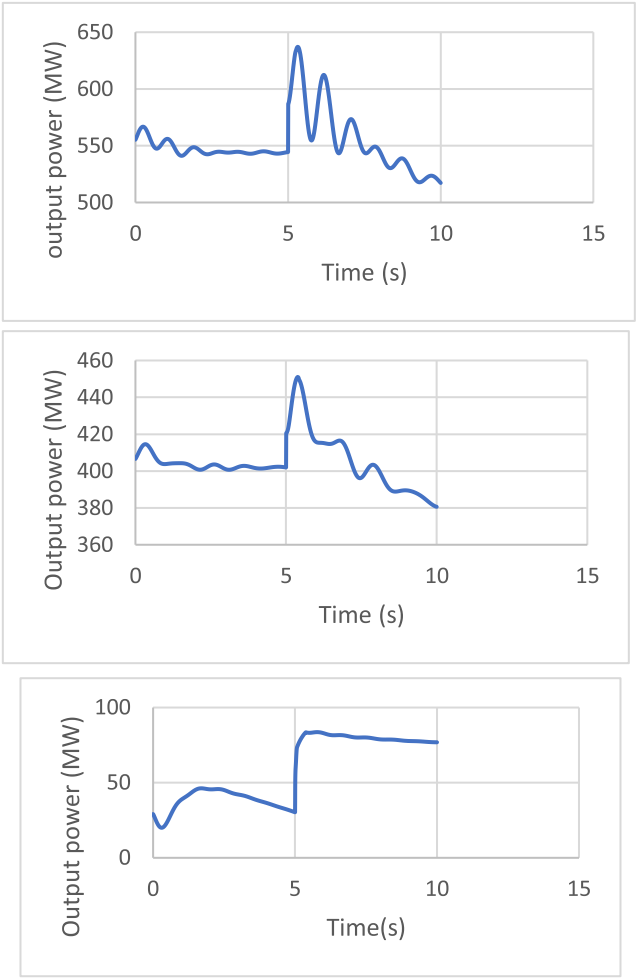

FIGURE 9. Active power injections (from G2, G3 and BESS top to bottom) during the sudden load increase of 300MW.

5 seconds after simulation started the BESS delivered an active power from 30MW to 83MW, releasing 53MW for inertial support. Fig. 9 also shows the active power outputs from the synchronous generators G2, G3, and BESS during the sudden load increase. Table 10 is a summary of the active power contributions from the synchronous generators and the BESS during the sudden load increase.

TABLE 10. Summary of the active powr contributions during the 300MW load increase.

Active power source	Released active power (MW) during the 300MW load increase
Generator 2	64.7
Generator 3	55.3
Battery energy storage (BESS)	31.4

TABLE 11. Summary of the RoCoF values for the modified 12-bus test system (after 300MW load increase).

Modified 12-bus test system	RoCoF (Hz/s)
With BESS working	-0.468
With BESS inactive	-0.613

2) RATE OF CHANGE OF FREQUENCY (ROCOF)

The rate of change of frequency (RoCoF) is another indicator of the frequency response of a system. The value gives insights regarding how the system frequency rises or falls during load/generator contingency event. According to the grid code from ENTSO-E [28], RoCoF protection relay should not be greater than 0.5Hz/s. In this work, the RoCoF for the simulation evaluation is computed as an average value of the derivation in a period between 0 to 200milliseconds after the sudden load increase of 300MW. For this work, the value of RoCoF obtained for the modified network when the BESS is working and when it is inactive are −0.468Hz/s and −0.613Hz/s respectively. These values show that when the BESS is inactive, the value of the RoCoF is higher, resulting in the frequency falling rapidly during the load event as compared to when the BESS is working. The values of the RoCoF during the load increase of 300MW are summarized in Table 11.

B. EFFECTS OF USING BESS FOR ADDITIONAL INERTIA SUPPORT DURING A SUDDEN LOSS OF 410MVA GENERATING UNIT ON THE SYSTEM

In this scenario, the use of BESS for additional inertia support and frequency improvement in the test model during a sudden loss of a generating unit is investigated. The generating unit, G3 (474 MVA) was delivering an active power of about 403MW and 74Mvar to the power network prior to the contingency which occurred at 5seconds after the commencement of the simulation. The active power output of G3 during the 10 seconds simulations is shown in Fig. 10 while Fig. 11 shows the frequency plots (with and without BESS) during the sudden outage. The release of active power from the BESS helped in keeping the minimum frequency at 48.44Hz, whereas without the BESS, the frequency fell to 47.79Hz. The graphs of the active power injections from the synchronous generator G2 and BESS (during the generation outage contingency) are shown in Fig. 12 and the actual values of active power injected are summarised in Table 12 while Table 13 is a summary of the system minimum frequencies during the outage of G3.

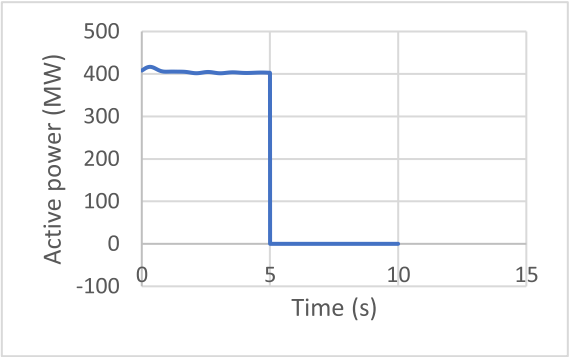

FIGURE 10. G3 output active power (before and after outage).

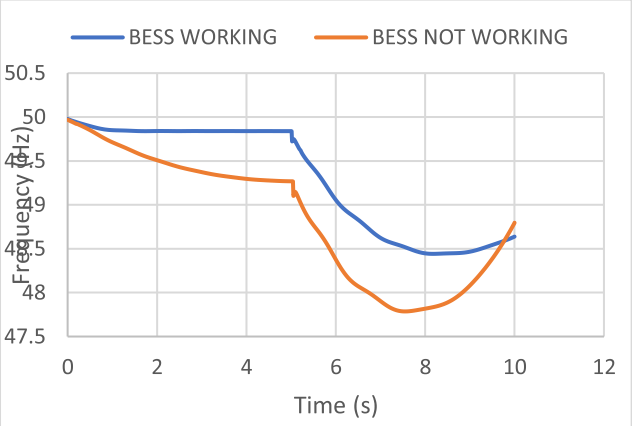

FIGURE 11. Frequency plots (with and without BESS) during the sudden outage of G3.

TABLE 12. Summary of the active powr injections during the outage of G3.

Active power sources	Active power injected during outage (MW)
G2	128
BESS	26

TABLE 13. Summary of the system frequency during the outage of G3.

Modified 12-bus system	Minimum system frequency (Hz)
With BESS	48.44
Without BESS	47.79

C. USING BESS FOR FREQUENCY SUPPORT DURING A SUDDEN LOAD DECREASE (LOSS OF 300MW LOAD)

In this test study, the impacts of BESS on frequency during a power system over frequency disturbance is investigated. A sudden load decrease of 300MW was activated in the test

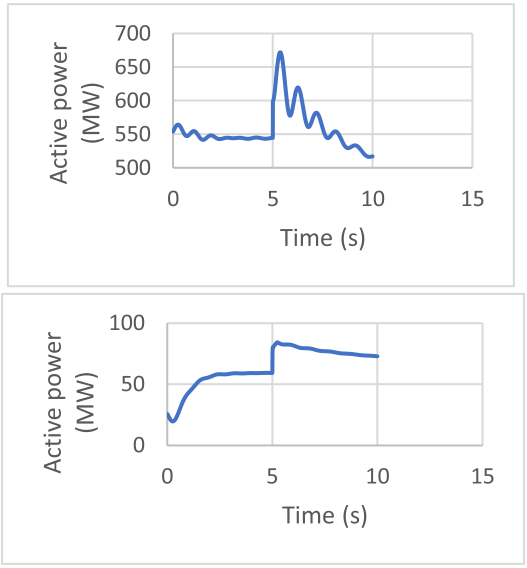

FIGURE 12. Active power injections (G2 (TOP) and BESS, (bottom)) during the sudden outage of G3.

network 5seconds after the commencement of the simulation (without and with BESS providing necessary frequency support). The whole simulation lasted for 10seconds. At 5seconds after the start of the simulation, due to the sudden load decrease of 300MW, the balance between the generation and the load was lost and the generation became higher than the load and then BESS began a charging operation. Consequently, the system frequency rises as clearly seen in the frequency plot shown in Fig 13a.

Through the operation of the frequency controllers, the BESS starts a charging process and absorb energy from the grid, thereby helping in keeping the frequency from rising above limits. Examining this test scenario with that studied in Section VI (subsection A), the effectiveness of BESS in keeping the system frequency within limits during both underfrequency and over frequency contingency events is clearly demonstrated. In the case of the underfrequency event (see Section VI, subsection A), at the sudden load increase of 300MW, the BESS discharges active power into the grid, thereby keeps the frequency from falling blow the limits that may activate underfrequency loadshedding. For the sudden load decrease of 300MW, the BESS, through its charging process absorbs about 96MW from the grid (see the active output power plots for BESS and the synchronous generators Fig 13b – Fig13d). With this power absorbed from the grid, the system frequency at the end of the 10 seconds after simulation was 50.94Hz. However, without BESS providing useful inertia support during contingency, the frequency at end of the 10seconds simulation was 51.52Hz. This may lead to over frequency loadshedding if not properly addressed. Table 14 is a summary of the system frequencies attained during the 10seconds simulations for 300MW load decrease with the BESS in operation and without the service of the

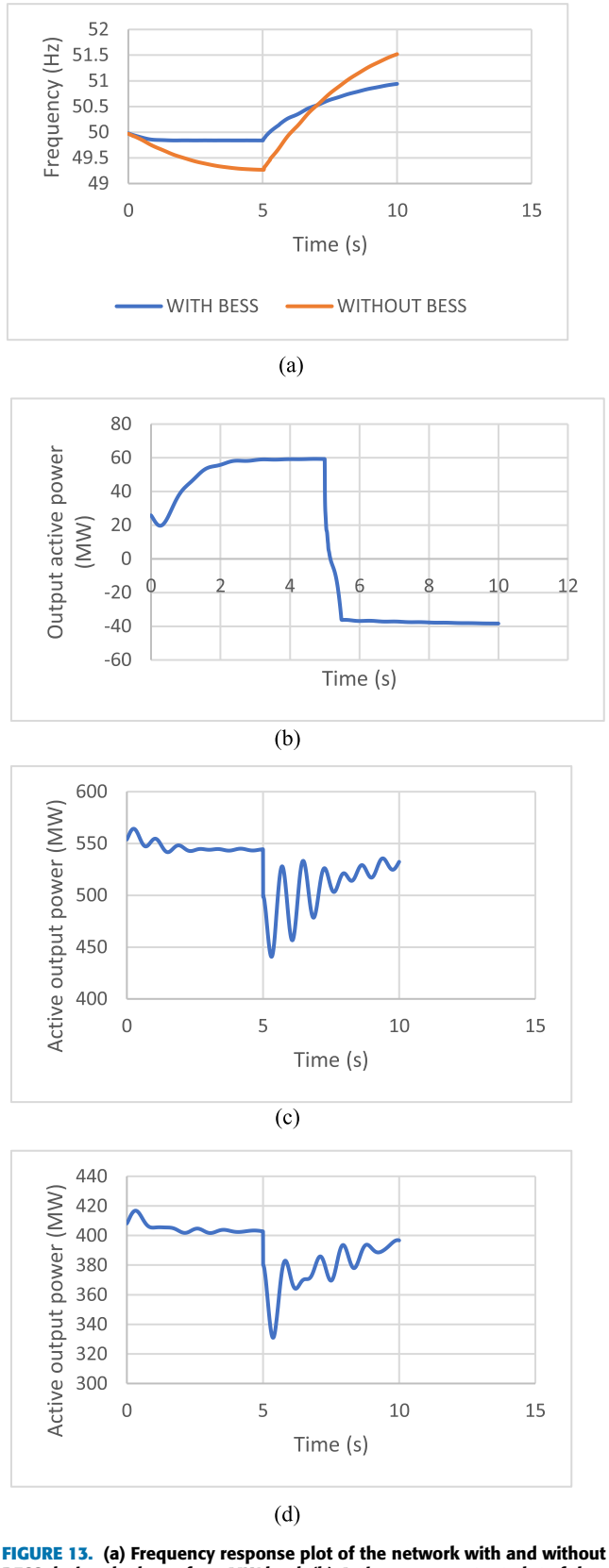

FIGURE 13. (a) Frequency response plot of the network with and without BESS during the loss of 300MW load. (b) Active power output plot of the BESS during the loss of 300MW load. (c) Active power output plot of G2 during the loss of 300MW load. (d) Active power output plot of G3 during the loss of 300MW load.

TABLE 14. Summary of the system frequencies during the loss of 300MW load.

Modified 12-bus system	Frequency (Hz)
With BESS	50.94
Without BESS	51.52

TABLE 15. Summary of the active power drawn from the grid during the loss of 300MW load.

Active power sources	Active power drawn (MW)
BESS	96
G2	103
G3	72

TABLE 16. Summary of the frequency nadirs of the network having different sizes of BESS.

BESS size (MW)	RoCoF (Hz/s)	Minimum frequency (Hz)
50	-0.43876	48.98
70	-0.38039	49.20
90	-0.35920	49.32
110	-0.33778	49.44
130	-0.30668	49.67

BESS. The summary of the active power absorbed from the grid by BESS and the synchronous generators are presented in Table 15.

D. EFFECTS OF BESS SIZE ON THE SYSTEM INERTIA AND FREQUENCY DURING CONTINGENCY

In this section, the impacts of BESS size on synthetic inertia and frequency during contingency are investigated. According to [29], grid-scale BESS with capacity greater than 50MW placed on transmission network has the potential to provide quick (in milliseconds) standby power sources to meet up demand and to absorb electricity at a time when its production is more than the demand. For this study, several sizes of BESS are chosen ranging from 50MW to 130MW in a step increase of 20MW. Contingency event of sudden load increase of 300MW) was activated and impacts of BESS size on the grid inertia and frequency were studied. The test system was simulated for 10 seconds. A load increase of 300MW was activated with different sizes of BESS ranging from 50MW to 130MW at 5 seconds from the commencement of the simulation for each size of BESS. Fig 14 presents the frequency plots for the simulation for the different sizes of BESS and Table 16 gives the summary of the RoCoF and frequency nadirs during the load increase contingency.

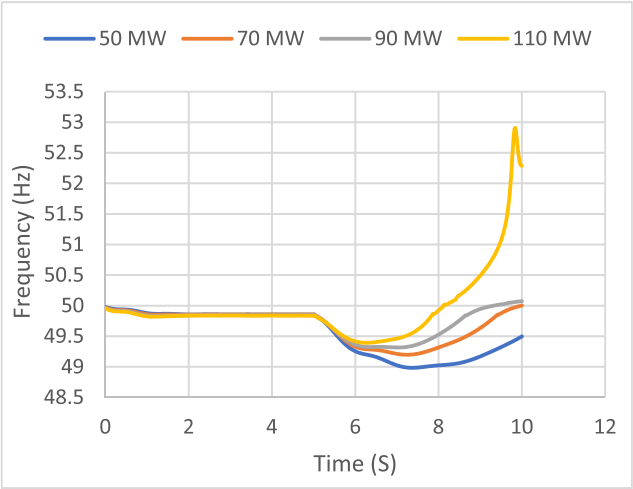

FIGURE 14. Frequency response plot of the network with different BESS sizes providing inertia support.

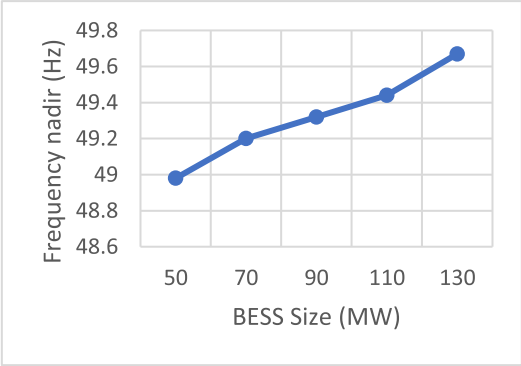

FIGURE 15. A plot of frequency nadirs and BESS sizes.

From the simulation results obtained, there is approximately a linear relationship between the size of BESS and the magnitude of the frequency nadir attained during the load increase contingency (see Fig 15). Consequently, signifying that as the size of BESS increases from 50MW to 130MW, for the 300MW sudden load increase the rate of change of frequency, RoCoF decreases and being inversely proportional to the system inertia according to the swing equation, more inertia is released during the disturbance event and the frequency nadir is improved from 48.98Hz to 49.67Hz. The increase in the frequency nadir is because of the additional provision of inertia from increasing the BESS capacity. Though, increasing the size of BESS capacity makes room for more inertia to be injected (to compensate for power deficit during contingency) but it also increases the cost of the BESS. Therefore, there may be need to consider using the BESS for multi-purpose applications.

However, it should be noted that the rise in frequency after about 9 seconds from the commencement of simulation was because the primary frequency reserve was not provided to restore the system to steady state frequency since our focus is on the inertia response.

E. EFFECTS OF TRANSMISSION LINE LENGTH ON THE FREQUENCY RESPONSE DURING THE 300MWLOAD INCREASE

In this instance, the effects of the transmission line lengths on the frequency response of a power system during a sudden load increase of 300MW is investigated. The purpose of this investigation is to ascertain if during power system contingency, the length of a transmission line has any effect on the inertia contribution from BESS. The length of the transmission lines is varied in three different scenarios (as shown in Table 18) and in each case, a sudden load increase of 300MW is activated using the load event contingency in the DIgSilent Power Factory. After each load increase event, the minimum frequency and the RoCoF are obtained. It should be noted that the RoCoF is taken as the average of the rate of change of frequency for 200ms from the instant of the contingency as shown in Table 17 while Table 18 shows the summary of the values of the various frequency response indicators. Fig. 16 – Fig. 17 are the frequency response curves for the investigated scenarios.

From Table 18, it is also clearly seen that when the transmission line lengths were increased, the values of the RoCoFs were lower and consequently the higher the values of the minimum frequencies. Therefore, the effectiveness of the BESS in providing inertia support for frequency stability for longer transmission lines is minimal. The lower values of the RoCoF for longer transmission lines could be explained based on the magnitude of the active power released by the synchronous generators and BESS at the instant of the sudden load increase. It should be noted that the longer the transmission line, the higher the value of the line reactance (line reactance is proportional to transmission line length) and this reduces the active power transferred from the output of the power converter (in ac power transfer, the power transferred is inversely proportional to the line reactance). Thus, when the transmission line is long, the line reactance is more and consequently the active power transferred is low. This means that the available active power from the BESS and the synchronous generators (G1 and G2) to compensate for the load increase is low as shown in Table 11. Thus, the net effect of this power on the power imbalance will result in a lower value of the rate of change of frequency restraining the frequency from falling deeper.

A sample calculation for the total active power injected by BESS, G2 and G3 within the 200ms load increase for a transmission length of "L" is shown in Table 19. DBESS is the power injected by BESS between two consecutive time intervals, DG2 is the power injected by generator 2 between two-time intervals and DG3 is the power injected by G3 between two-time intervals.

F. EFFECTS OF THE MAGNITUDE OF SUDDEN CHANGE IN LOAD DEMAND ON FREQUENCY RESPONSE

This test scenario shows the response of the system frequency to sudden change in the magnitudes of load increase. Ten contingency events of load increase from 30MW to 375MW were investigated. Two frequency response indicators namely minimum frequency and RoCoF were used to study the response of the modified 12-bus system under these contingencies. In Table 20, ΔP_L is the sudden increase in load, $P_{O(PC)}$ is the output active power from the power converter (released

TABLE 17. Sample of RoCoF calculation for transmission line length "L" km.

Time(s)	Frequency (Hz)	df/dt (Hz/s)
5.0001	49.936509	
5.0051	49.936576	0.0134
5.01167	49.93661	0.0051
5.02167	49.885795	-5.0815
5.03167	49.885161	-0.0634
5.04167	49.887653	0.2492
5.05167	49.889154	0.1501
5.06167	49.888314	-0.0841
5.07167	49.885772	-0.2542
5.08167	49.882089	-0.3683
5.09167	49.877223	-0.4866
5.10167	49.871656	-0.5567
5.11167	49.866246	-0.5411
5.12167	49.861033	-0.5213
5.13167	49.85598	-0.5053
5.14167	49.851035	-0.4945
5.15167	49.846164	-0.4871
5.16167	49.841346	-0.4818
5.17167	49.836574	-0.4772
5.18167	49.831844	-0.473
5.19167	49.827159	-0.4685
5.20167	49.82252	-0.4639
	ROCOF	-0.5424

TABLE 18. Summary of the active power delivery from the BESS, G2, and G3 and their corresponding frequency response values under different transmission line lengths.

Line lengths(km)	Total active power from (BESS, G2 and G3)	Minimum frequency (Hz)	RoCoF (Hz/s)
L	145.36	49.39	-0.5424
1.5L	126.29	49.73	-0.3268
2.0 L	100.40	49..85	-0.1304

Note: L is the original length of the transmission line given in Table III, therefore, 1.5L means that the transmission line length is increased to 1.5 times the initial length.

TABLE 19. A sample calculation of the total active power injected by BESS, generator 2 and generator 3.

TIME (S)	BESS (MW)	G2 (MW)	G3 (MW)	DBESS (MW)	DG2 (MW)	DG3 (MW)
5.000001	402.574	542.921	24.477			
5.005001	421.420	584.019	44.497	18.846	49.098	20.020
5.011667	422.014	583.578	54.325	0.594	-0.441	9.828
5.021667	422.277	583.484	58.446	0.263	-0.093	4.120
5.031667	422.537	583.608	61.195	0.260	0.123	2.749
5.041667	422.792	583.758	64.406	0.254	0.150	3.212
5.051667	423.137	584.111	67.014	0.345	0.353	2.608
5.061667	423.572	584.624	69.376	0.435	0.513	2.362
5.071667	424.101	585.302	71.423	0.530	0.678	2.047
5.081667	424.754	586.215	72.559	0.653	0.913	1.136
5.091667	425.516	587.322	73.017	0.763	1.107	0.458
5.101667	426.341	588.508	73.554	0.825	1.186	0.537
5,111667	427.220	589.771	74.055	0.879	1.262	0.501
5.121667	428.143	591.091	74542	0.923	1.320	0.487
5.131667	429.102	592.457	75.013	0.959	1.365	0.471
5.141667	430.090	593.853	75.467	0.988	1.397	0.455
5.151667	431.099	595.269	75.908	1..009	1.416	0.440
5.161667	432.123	596.691	76.333	1.024	1.422	0.426
5.171667	433.155	598.107	76.745	1.032	1.416	0.412
5.181667	434.189	599.505	77.144	1.034	1.399	0.399
5.191667	435.219	600.875	77.531	1.030	1.370	0.386
5.201667	436.240	602.206	77.905	1.021	1.331	0.374
			TOTAL	32.645	59.285	53.428
	Total power injected by BESS, G2 and G3=145.36MW.					

by BESS at the instant of the sudden load increase) F_{MIN} is the minimum frequency of the system because of the sudden increase in load and RoCoF is the rate of change of frequency with respect to time because of the sudden increase in load. Results from the simulations clearly show that the size of the power imbalance has a direct and significant effect on the grid frequency which agrees with [1]. That is, as the magnitude of the power disturbances increases the RoCoF also increases and consequently, the frequency falls deeper. It is also important to note that as the size of the power imbalance increases, the power injected by the BESS, that is $P_{O(PC)}$ also increases

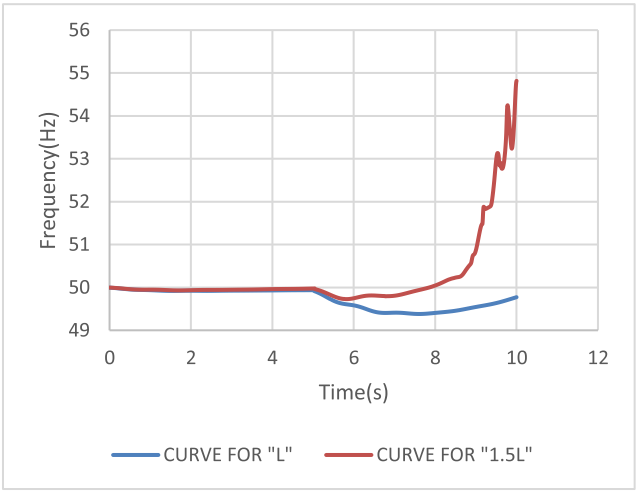

FIGURE 16. Frequency response curve (with transmission line "L" km and 1.5L for 300MW load increase.

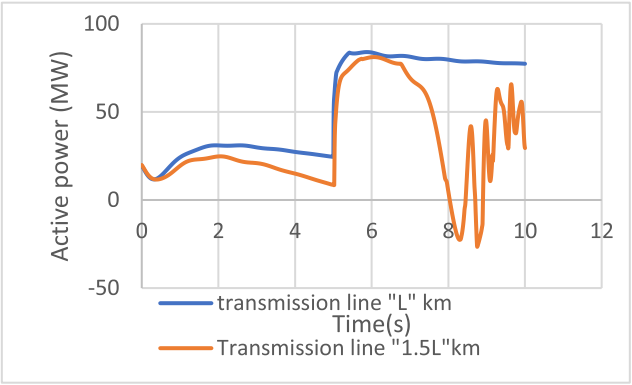

FIGURE 17. A curve of active power delivery from BESS (when the transmission line length of "L" and "1.5L" for 300MW load increase.

until it reaches its maximum value of about 62.4 MW and then declines (see Table 20 and Fig 10) This shows that once the maximum output power of the power converter is reached (about 62.4MW in this study) further increase in the size of the disturbance will not result in an increase in the active power injected by the BESS. Therefore, at that level the BESS will not be effective in managing the frequency deviations resulting from any further sudden increase in the load. The graph showing the relationship between the sizes of disturbances (in MW) and the corresponding output power of the power converter (in MW) is shown in Fig 18.

G. EFFECTS OF THE VARITION IN THE WIND OUTPUT POWER ON THE ADDITIONAL INERTIA SUPPORT FROM BESS

One of the challenges in the use of wind and solar photovoltaic as renewable energy sources of generation of electricity is their dependency on weather for power generation. Thus, the output power production is variable. This test study investigates the effects of the intermittency of power generation from wind power plants on the inertia contribution

TABLE 20. A summary of frequency response during sudden increase in load.

ΔP_L(MW)	$P_{O(PC)}$ (MW)	RoCoF (Hz/s)	F_{MIN} (Hz)
30	14.74	-0.11135	49.91
75	44.16	-0.13478	49.83
105	62.36	-0.15843	49.79
150	62.05	-0.22734	49.70
180	61.57	-0.27307	49.62
225	60.78	-0.33868	49.52
255	60.62	-0.38122	49.46
300	59.67	-0.44773	49.38
330	59.03	-0.49401	49.34
375	58.56	-0.56223	49.29

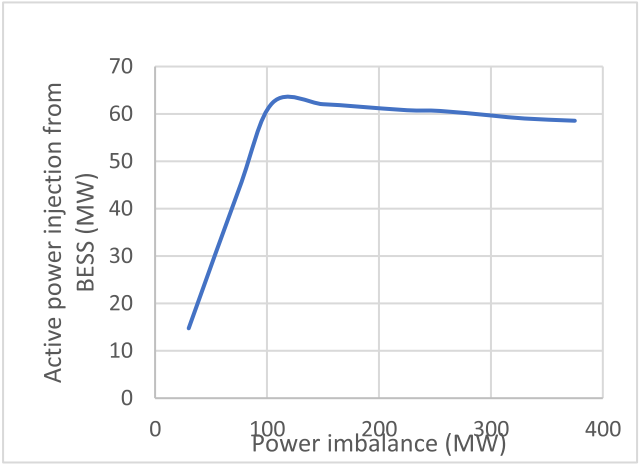

FIGURE 18. A graph showing the relationship between the active power injected by BESS (MW) and power imbalance (MW).

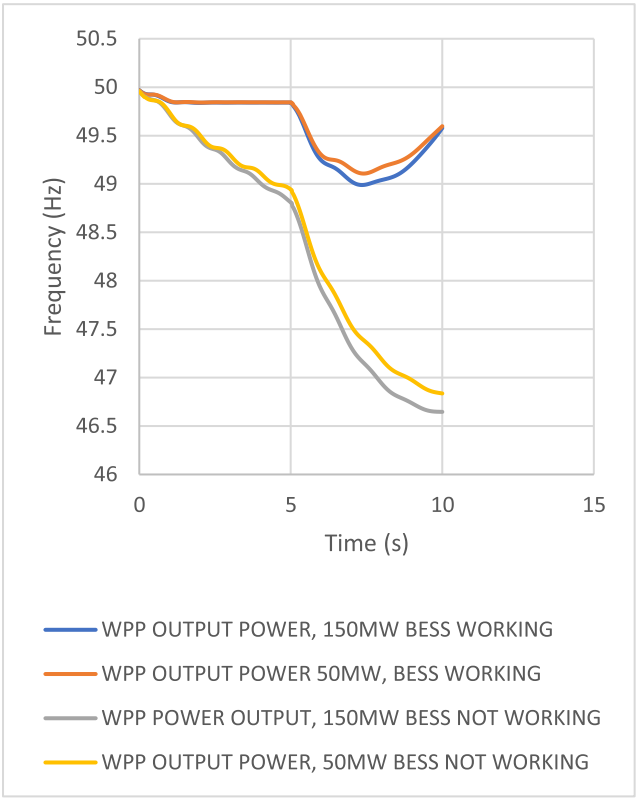

FIGURE 19. Frequency response plot for WPP with variable power output during system disturbance.

from BESS during power system disturbance event. The test model (Fig 7) has two WPPs. For this investigation, the output power from each of the WPP is considered to vary from 50MW to 150MW in steps of 20MW. For each output power from the WPPs, the test system is simulated and a sudden load increase of 300MW is activated after five seconds from the commencement of the simulation for each of the power output from the WPPs, two scenarios are considered: BESS providing inertia support during contingency and BESS not providing inertia support. Presented in the simulation results are presented in Table 21.

The results show that the variableness of the output power from the WPPs does not affect the frequency nadir during the contingency. When the test system has BESS working, the frequency nadir was approximately 49Hz during the load increase contingency. The minimum frequency did not show appreciable change as the output power from the WPPs varies between 50MW to 150MW. The same also applies for the case when BESS was not working in the test system. The minimum frequency was about 47Hz as the output power changes from 50MW to 150MW. These agree with the literature that WPPs do not naturally account for the overall grid inertia during frequency events except when they are specifically controlled to provide such, for example by using the methodology of maximal power point tracking (MPPT). The system frequency nadir fell to about 47Hz when BESS was not working but rose to about 49Hz when BESS was connected to the test system. The results showed the effectiveness of BESS in the provision of additional inertia support during frequency event. In Fig 19, the frequency response is compared for the maximum and minimum power output from the WPP (with and without the BESS). When the BESS was working, the minimum frequency was almost the same though the power output from the WPP was 50MW and 150MW. The plots of the active power injected by the CPPs and BESS during the load increase contingency for 50MW power output generation from WPP1 are presented in Fig 20a to Fig 20c. Fig20d shows that no active power was injected by WPP1 at the instant of the load increase contingency while Fig 20e shows a similar case of no power injection for WPP2 during contingency.

H. EFFECTS OF SUDDEN LOAD INCREASE OF 300MW UNDER VARYING GRID INERTIA

The power system grid inertia refers to the stored kinetic energy of the rotating masses of the synchronous generators

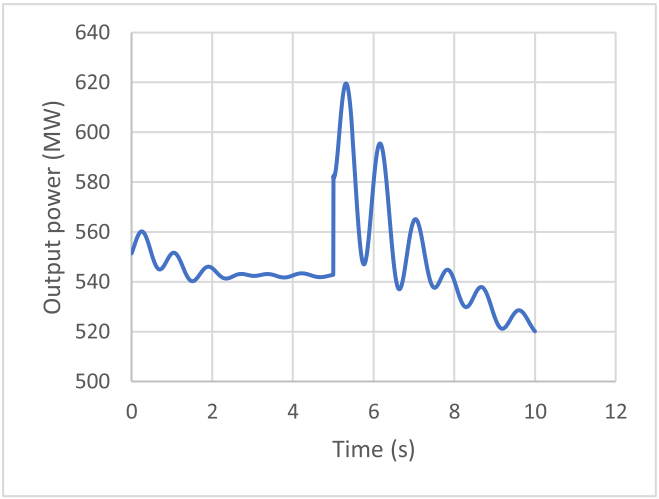

(a)

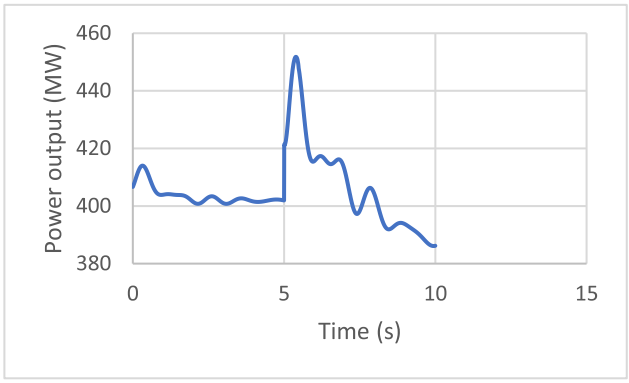

(b)

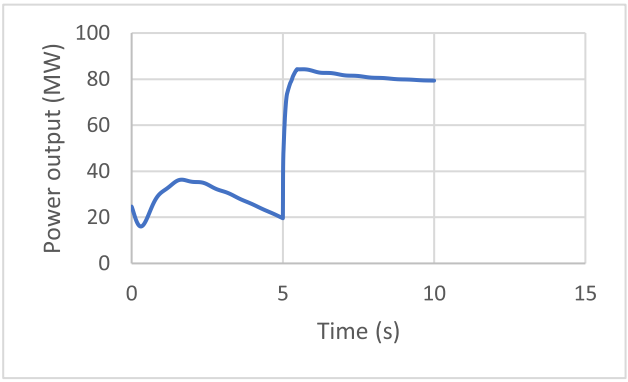

(c)

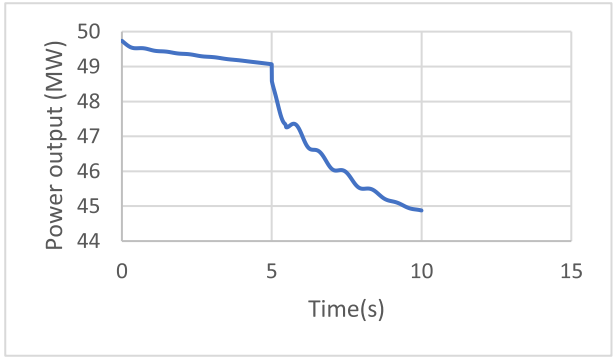

(d)

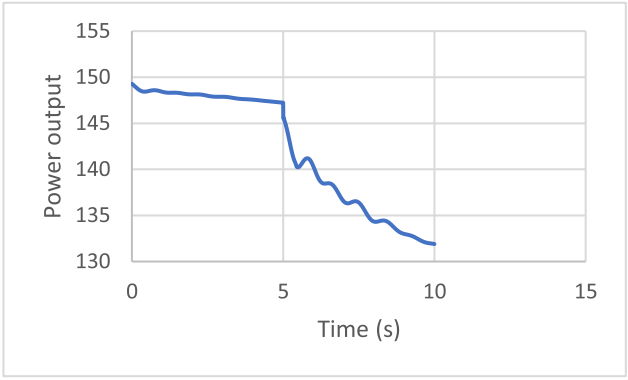

(e)

FIGURE 20. (a) Power(active) injection by the synchronous generator G2 during the load increase contingency (WPPS delivering an output power of 50MW each). (b) Power(active) injection by the synchronous generator G3 during the load increase contingency (WPPS delivering an output power of 50MW each). (c) Power(active) injection by the BESS during the load increase contingency (WPP delivering an output power of 50MW each). (d) WPP1 Injecting no active power at the instant (5s) of load increase contingency. (e) WPP2 Injecting no active power at the instant (5s) of load increase contingency.

and motors connected to it [30], [31], [32], [33], [34]. To study the effects of sudden load increase on varying grid inertia, the inertia of the grid network is varied by decreasing the number of the synchronous-based power plants at

TABLE 21. Frequency nadirs for the test system during 300MW load increase contingency (WPP delivering variable power output).

Variable Power output from WPP (MW)	Minimum frequency (BESS not working) (Hz)	Minimum frequency (BESS working) (Hz)
50	46.84	49.11
70	46.80	49.08
90	46.76	49.03
110	46.72	49.02
130	46.69	49.00
150	46.66	48.99

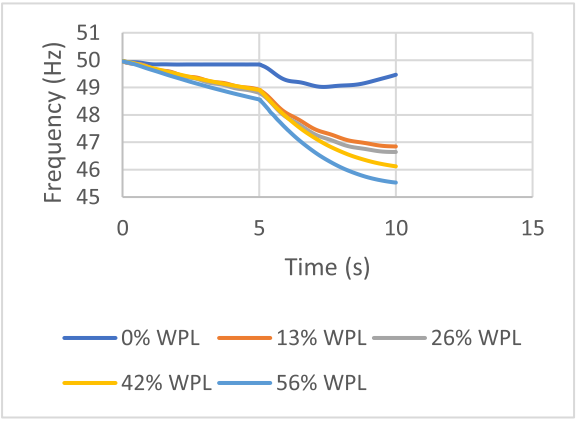

FIGURE 21. Frequency response plots for different wind penetration levels (varying grid inertia) BESS not working.

the same time increasing the number of the wind power plants. Thus, as the penetration of the wind power generation increases, its grid inertia is varied. For this test scenario, five different wind penetration levels (WPLs) are considered. Each value of WPL (in percentage) is evaluated based on the wind generation (MW) with respect to the total generation (MW) of the test model (that is, [wind generation/total generation] x 100). The test model under each WPL is activated for a load increase contingency after 5s from the commencement of simulation. The simulations are run for 10 seconds, and two conditions of the network are investigated, (1) the network has no additional inertia form BESS and (2) the network has additional inertia from BESS. The frequency plots are shown in Fig. 21 and Fig. 22 while the results are summarised in Table 22.

The simulation results show that as the wind penetration level increases (thereby varying the grid inertia), the rate of change of frequency (RoCoF) increases during the load

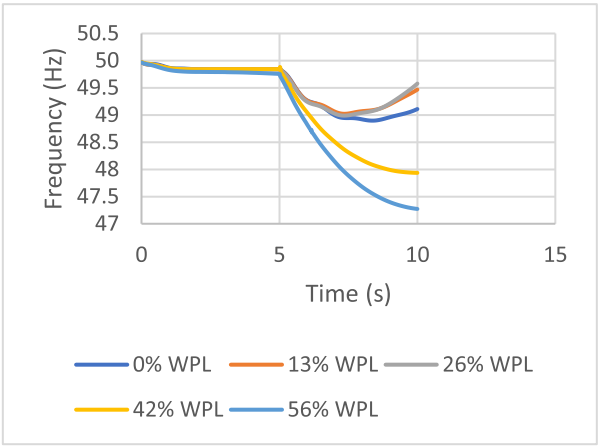

FIGURE 22. Frequency response plots for different wind penetration levels (varying grid inertia) BESS working.

TABLE 22. Effects of a sudden 300MW increase in load under varying grid inertia.

Wind penetration level (%) (Varying grid inertia)	RoCoF (Hz/s) Without BESS	F_{min} in Hz) With out BESS	RoCoF (Hz/s) With BESS	F_{min} (Hz) With BESS
0	-0.5212	48.55	-0.3456	49.55
13	-0.8012	46.84	-0.3934	49.02
26	-0.8097	46.66	-0.4258	48.99
42	-1.0766	46.10	-0.8195	47.93
56	-1.7035	45.52	-0.9586	47.27

increase contingency. The increase in the RoCoF will cause the frequency nadir to fall in such a way that if not addressed, may trigger under frequency load shedding. At the wind penetration levels of 13% and 26%, with the BESS giving additional inertia, the RoCoF values (see Table 22) were about 50% lower than the values obtained when BESS was not working. The additional inertia supplied by BESS helped in sustaining the frequency nadir to about 49Hz.

However, when the WPL increased to 42% and 56%, the BESS could not effectively supply enough inertia to address the rise in the rate of change of frequency (RoCoF). This resulted in the frequency nadir falling to a very low value of 47.27Hz (for the 56% WPL). One possible way of solving this problem is by increasing the size of the BESS and the converter capacity (as discussed in section V-E) correspondingly so that more inertia could be released during the contingency event. However, increasing the capacity of the BESS will also increase its cost and may result in more power losses in the network. Therefore, optimal sizing and placement of BESS is required for the full benefit of BESS installation to be realised. Moreso, further tuning of the active part of

the PQ controllers (K_p and T_{ip}) may be required for better frequency response and more active power provision by the BESS. Finally comparing the simulation results for the two conditions of the test network (that is with and without BESS), from Fig. 21 and Fig 22, the impact of BESS is also seen as it helped in maintaining the frequency close to 50Hz prior to contingency event in the varying grid inertia in the network.

VII. CONCLUSION

This work has demonstrated that BESS could be enabled through a frequency controller to provide inertia support during frequency contingency in a power system network. The various case studies investigated showed that transmission line lengths, magnitude of power imbalance, battery sizes, and varying grid inertia play significant roles in the effectiveness of BESS providing synthetic inertia support to a transmission network during power system contingencies.

Firstly, the results of this work showed that increasing the size of the BESS from 50MW to 130MW, the rate of change of frequency (RoCoF) was reduced from −0.43876Hz/s to −0.30668Hz/s and consequently the system frequency was improved from 48.98Hz to 49.67Hz. This agrees with the literature, that at a higher capacity of BESS more active power will be injected by the BESS to compensate for the power deficit during the contingency event. However, it should be noted that increasing the size of BESS may increase the power losses in the network if appropriate measures such as optimal sizing and placement of the BESS are not taken into consideration.

Besides, this study emphasized the significance of BESS for inertia support in a network of varying grid inertia. As the wind penetration level in the studied network increased from 13% to 56% (as a result of the replacement of the synchronous based power plant with the wind power plants), the rate of change of frequency (RoCoF) during the load increase contingency increased from −0.8012Hz/s to −1.7035Hz/s (without BESS) and as a result the system frequency fell from 46.84Hz to 45.52Hz respectively. However, with BESS providing additional inertia support, the rate of change of frequency (under the same study conditions) was from −0.3934Hz/s to −0.9586Hz/s with corresponding frequency range of 49.02Hz to 47.27Hz.This also, is in line with results of studies in the literature which confirm that as the wind penetration level increases in a network, the system inertia is reduced and if appropriate steps are not put into consideration (such as using BESS for additional inertia support) such a network may be prone to frequency instability on the event of power system disturbances.

Moreso, the impact of transmission line lengths on the effectiveness of BESS in providing frequency support during contingency was brought to light through this study. The results of this work showed that a longer transmission line has a lower RoCoF value when compared to a shorter transmission line when both lines are having the same loadings and are subjected to the same contingency event (sudden load increase). This is supported by the simulation results which revealed that when the transmission line lengths are doubled for the studied network, the rate of change of frequency (RoCoF) decreased by about 76% resulting in the system frequency increasing from 49.39Hz to 49.85Hz during the power system load increase of 300MW in the studied network. We would like to highlight that this should be taken into consideration in the sizing of a BESS for inertia support in a transmission network, in order to avoid over-sizing of the BESS because of the inherently low RoCoF of longer transmission lines.

Lastly, the investigation conducted in this work brought to light the ineffectiveness of BESS in providing inertia support once the converter maximum power is exceeded. It should be noted that there is a positive linear relationship between the magnitude of power imbalance and the active power injected by the BESS during sudden load increase contingency. That is as the power imbalance increases, the active power released by the BESS (to compensate for the power imbalance during load increase disturbance) via the power converter also increases. However, once the maximum power output of the converter is reached, further increase in the magnitude of the power imbalance will not result in a corresponding increase in the active power injected by the BESS. Which means that at the maximum power output of the power converter, the active power injected by the BESS remains fairly constant even when the magnitude of the disturbance is increased. This is extremely critical because at that level (when the maximum output power of the converter is attained) the active power injected by BESS will remain fairly constant despite further increase in the size of the disturbances, thus, becoming ineffective in providing additional inertia support to curtail frequency deviations. Therefore, it is necessary that the power converter capacity should be calculated based on the maximum size of the disturbance (that the network is designed to accommodate) and other system parameters rather than using only simulation convergence.

Thus, this study through the simulations and the results obtained has laid the foundation required for a BESS to be effective in providing additional inertia support in power system network with high renewal energy sources.

REFERENCES

[1] S. M. Alhejaj and F. M. Gonzalez-Longatt, "Impact of inertia emulation control of grid-scale BESS on power system frequency response," Presented at the Int. Conf. Students Appl. Eng. (ICSAE), Newcastle Upon Tyne, U.K., Oct. 2016.

[2] M. S. Alam, F. S. Al-Ismail, A. Salem, and M. A. Abido, "High-level penetration of renewable energy sources into grid utility: Challenges and solutions," *IEEE Access*, vol. 8, pp. 190277–190299, 2020.

[3] V. Knap, S. K. Chaudhary, D. Stroe, M. Swierczynski, B. Craciun, and R. Teodorescu, "Sizing of an energy storage system for grid inertial response and primary frequency reserve," *IEEE Trans. Power Syst.*, vol. 31, no. 5, pp. 3447–3456, Sep. 2016.

[4] H. Evelyn, T. Fei, and S. Goram, "Challenges and opportunities of inertia estimation and forecasting in low-inertia power systems," *Renew. Sustain. Energy Rev.*, vol. 147, pp. 1–12, Sep. 2021.

[5] P. Telens and D. V. Hertem, "Grid inertia and frequency control in power systems with high penetration of renewables," Presented at the Young Researcher Symp. Elect. Power Eng., Delft, The Netherlands, Jan. 2012.

[6] S. S. Alam, F. Saleh Al-Ismail, and M. A. Abido, "PV/wind-integrated low-inertia system frequency control: PSO-optimized fractional-order PI-based SMES approach," *Sustainability*, vol. 13, no. 14, pp. 1–21, Jul. 2021.
[7] W. Xing, H. Wang, L. Lu, X. Han, K. Sun, and M. Ouyams, "An adaptive virtual inertia control strategy for distributed battery energy storage system in microgrids," *Energy*, vol. 233, pp. 1–17, Oct. 2021.
[8] Z. Wu, D. W. Gao, H. Zhang, S. Yan, and X. Wang, "Coordinated control strategy of battery energy storage system and PMSG-WTG to enhance system frequency regulation capability," *IEEE Trans. Sustain. Energy*, vol. 18, no. 3, pp. 1330–1343, Jul. 2017.
[9] X. Li, Y. Huang, J. Huang, S. Tan, M. Wang, T. Xu, and X. Chang, "Modeling and control strategy for battery energy storage systems, for primary frequency regulation," Presented at the Int. Conf. Power Syst. Technol., Chengdu, China, Oct. 2014.
[10] R. Adamczyk, R. Teodorescu, and P. Rodriguez, "Adaptation of 12-bus system for wind power integration studies," in *Proc. 9 Int. Workshop Large Scale Integr. Wind Power Power Syst. Transmiss. Netw. Off-Shore Wind Power Plants*, Quebec, QC, Canada, Aug. 2010, pp. 821–825.
[11] S. M. Alhejaj and F. M. Gonzalez-Longatt, "Investigation on grid-scale BESS providing inertial response support," Presented at the IEEE Int. Conf. Power Syst. Technol., Wollongong, NSW, Australia, Oct. 2016.
[12] E. Robert, M. Niklas, and E. Katherine, "Synthetic inertia versus fast frequency response: A definition," *IET Renew. Power Gener.*, vol. 12, no. 5, pp. 507–514, Apr. 2018.
[13] M. Pieuluigui and B. Farhad, "The fragile grid: The physics and economics of security services in low-carbon power systems," *IEEE Power Energy Mag.*, vol. 19, no. 2, pp. 79–88, Mar./Apr. 2021.
[14] P. Kundur, N. Balu, and M. Lauby, *Power System Stability and Control*. London, U.K.: McGraw-Hill, 1994.
[15] S. Chen, T. Zhang, H. B. Gooi, R. D. Masiello, and W. Katzenstein, "Penetration rate and effectiveness studies of aggregated BESS for frequency regulation," *IEEE Trans. Smart Grid*, vol. 7, no. 1, pp. 167–177, Jan. 2016.
[16] A. Ter-Gezerian, *Energy Storage for Power Systems*. London, U.K.: Peter Peregium, 2012.
[17] H. Alsharif, M. Jalili, and K. N. Hasan, "Power system frequency stability using optimal sizing and placement of battery energy storage system under uncertainty," *J. Energy Storage*, vol. 50, Jun. 2022, Art. no. 104610.
[18] G. L. Francisco, "Frequency control and inertial response schemes for the future power networks," in *Large Scale Renewable Power Generation*. Singapore: Springer, 2014, pp. 193–231.
[19] A. P. Asensio, F. Gonzalez-Longatt, S. Arnaltes, and J. L. Rodríguez-Amenedo, "Analysis of the converter synchronizing method for the contribution of battery energy storage systems to inertia emulation," *Energies*, vol. 13, pp. 1478–1496, Mar. 2020.
[20] A. Shrestha and F. Gonzalez-Longatt, "Frequency stability issues and research opportunities in converter dominated power system," *Energies*, vol. 14, no. 14, pp. 4184–4212, Jul. 2021.
[21] U. Tamrakar, D. Shrestha, M. Maharjan, B. P. Bhattarai, T. Hansan, and R. Tonkoski, "Virtual inertia: Current trends and future directions," *Appl. Sci.*, vol. 7, no. 7, pp. 654–683, Jun. 2017.
[22] F. M. Gonzalez-Longatt, "Effects of fast acting power controller of BESS in the system frequency response of a multi-machine system: Probabilistic approach," Presented at the Int. Conf. Innov. Smart Grid Technol., Singapore, May 2018.
[23] M. N. Acosta, F. Gonzalez-Longatt, S. Denysiuk, and H. Strelkova, "Optimal settings of fast active power controller: Nordic case," Presented at the IEEE 7th Int. Conf. Energy Smart Syst., Kyiv, Ukraine, May 2020.
[24] E. Rakhshani, A. Perilla, J. L. R. Torres, F. M. Gonzalez-Longatt, T. B. Soeiro, and M. A. M. M. Van Der Meijden, "FAPI controller for frequency support in low-inertia power systems," *IEEE Open Access J. Power Energy*, vol. 7, pp. 276–286, 2020.
[25] N. Mirza and Y. Guangya, "Battery energy storage system modelling in DIgSILENT PowerFactory," in *Modelling and Simulation of Power Electronic Converter Dominated Power Systems in PowerFactory*. Switzerland: Springer, 2021.
[26] *Battery Energy Storage System (BESS) Model*, DIgSILENT Power Factory Manual, Gomaringen, Germany, 2010.
[27] C. K. Das, T. S. Mahmoud, O. Bass, S. M. Muyeen, G. Kothapalli, A. Baniasadi, and N. Mousavi, "Optimal sizing of a utility-scale energy storage system in transmission networks to improve frequency response," *J. Energy Storage*, vol. 29, pp. 1–22, Jun. 2020.
[28] *Supporting Documents for Network Code on Load-Frequency Control and Reserves*, ENTSOE, Brussels, Belgium, 2013.
[29] F. M. Gonzalez-Longatt and S. M. Alhejaj, "Enabling inertial response in utility-scale battery energy storage system," Presented at the IEEE Innov. Smart Grid Technol., Melbourne, VIC, Australia, Nov. 2016.
[30] F. M. Gonzalez-Longatt, A. Bonfiglio, R. Procopio, and B. Verduci, "Evaluation of inertial response controllers for full-rated power converter wind turbine (type 4)," Presented at the IEEE PES Gen. Meeting, Boston, MA, USA:, Jul. 2016.
[31] F. M. Gonzalez-Longatt, J. L. Rueda, and E. Vazquez, "Effect of fast acting power controller of battery energy storage systems in the under-frequency load shedding scheme," in *Proc. Int. Conf. Innov. Smart Grid Technol.*, Singapore, Jun. 2018, pp. 1–6.
[32] F. M. Gonzalez-Longatt, J. M. Roldan-Fernandez, H. R. Chamorro, S. Arnaltes, and J. L. Rodriguez-Amenedo, "Investigation of inertia response and rate of change of frequency in low rotational inertial scenario of synchronous dominated system," *Electronics*, vol. 10, no. 18, pp. 1–24, Sep. 2021.
[33] P. Wall, F. Gonzalez-Longatt, and V. Terzija, "Estimation of generator inertia available during a disturbance," Presented at the IEEE Power Energy Soc. Gen. Meeting, San Diego, CA, USA, Jul. 2012.
[34] M. J. Rainey and D. T. O. Oyedokun, "Transmission line damping effects on power system inertia response," Presented at the Int. SAUPEC/Robmec/PRASA Conf., Cape Town, South Africa, Jan. 2020.

CHUKWUEMEKA E. OKAFOR received the B.Eng. degree in electrical engineering from the University of Nigeria, in 1998, and the M.Eng. degree in power and machines from the University of Benin, Benin, Nigeria, in 2006. He is currently pursuing the Ph.D. degree in electrical engineering with the University of Cape Town, Cape Town, South Africa.

He was a Lecturer with the Department of Electrical and Electronic Engineering, Ekiti State University, Ado-Ekiti, Nigeria, for over ten years. His research interests include renewable energy, energy storage, power system stability, and power system optimization.

KOMLA A. FOLLY (Senior Member, IEEE) received the B.Sc. and M.Sc. degrees in electrical engineering from Tsinghua University, Beijing, China, in 1989 and 1993, respectively, and the Ph.D. degree in electrical engineering from Hiroshima University, Japan, in 1997. From 1997 to 2000, he was with the Central Research Institute of Electric Power Industry (CRIEPI), Tokyo, Japan. He is currently a Professor with the Department of Electrical Engineering, University of Cape Town, Cape Town, South Africa. In 2009, he received the Fulbright Scholarship and was a Fulbright Scholar at the Missouri University of Science and Technology, Rolla, MO, USA. His research interests include power system stability, control, and optimization, HVDC modeling, grid integration of renewable energy, application of computational intelligence to power systems, smart grids, and power system resilience. He is a member of the Institute of Electrical Engineers of Japan (IEEJ) and a fellow of the SAIEE.